Investigating the structural plasticity of a cytochrome P450: three-dimensional structures of P450 EryK and binding to its physiological substrate.

Carmelinda Savino, Linda C Montemiglio, Giuliano Sciara, Adriana E Miele, Steven G Kendrew, Per Jemth, Stefano Gianni, Beatrice Vallone

THE JOURNAL OF BIOLOGICAL CHEMISTRY VOL. 284, NO. 42, pp. 29170–29179, October 16, 2009

Investigating the Structural Plasticity of a Cytochrome P450

THREE-DIMENSIONAL STRUCTURES OF P450 EryK AND BINDING TO ITS PHYSIOLOGICAL SUBSTRATE[*][S]

Received for publication, April 3, 2009, and in revised form, July 15, 2009 Published, JBC Papers in Press, July 22, 2009, DOI 10.1074/jbc.M109.003590

Carmelinda Savino[‡§1], Linda C. Montemiglio[§1], Giuliano Sciara[§2], Adriana E. Miele[§], Steven G. Kendrew[¶], Per Jemth[‖], Stefano Gianni[‡§3], and Beatrice Vallone[§4]

From the [‡]CNR Institute of Molecular Biology and Pathology, P.le A. Moro 5, 00185 Rome, Italy, the [§]Department of Biochemical Sciences, "Sapienza" University of Rome, P.le A. Moro 5, 00185 Rome, Italy, [¶]Biotica Technology Ltd., Chesterford Research Park, Little Chesterford, Saffron Walden, Essex CB10 1XL, United Kingdom, and the [‖]Department of Medical Biochemistry and Microbiology, Uppsala University, BMC Box 582, SE-75123 Uppsala, Sweden

Cytochrome P450s are heme-containing proteins that catalyze the oxidative metabolism of many physiological endogenous compounds. Because of their unique oxygen chemistry and their key role in drug and xenobiotic metabolism, particular attention has been devoted in elucidating their mechanism of substrate recognition. In this work, we analyzed the three-dimensional structures of a monomeric cytochrome P450 from *Saccharopolyspora erythraea*, commonly called EryK, and the binding kinetics to its physiological ligand, erythromycin D. Three different structures of EryK were obtained: two ligand-free forms and one in complex with its substrate. Analysis of the substrate-bound structure revealed the key structural determinants involved in substrate recognition and selectivity. Interestingly, the ligand-free structures of EryK suggested that the protein may explore an open and a closed conformation in the absence of substrate. In an effort to validate this hypothesis and to investigate the energetics between such alternative conformations, we performed stopped-flow absorbance experiments. Data demonstrated that EryK binds erythromycin D via a mechanism involving at least two steps. Contrary to previously characterized cytochrome P450s, analysis of double jump mixing experiments confirmed that this complex scenario arises from a pre-existing equilibrium between the open and closed subpopulations of EryK, rather than from an induced-fit type mechanism.

The cytochrome P450 (P450) family consists of heme-containing enzymes with extremely diverse functions, distributed in virtually all organisms, from bacteria to human (1). They catalyze the oxidation of non-reactive C-H bonds and are involved in numerous metabolic reactions of many physiological endogenous compounds (*i.e.* antibiotics, lipids, and steroids), as well as xenobiotic molecules (2–4). Because of their unique oxygen chemistry and key role in drug metabolism, multidisciplinary research has been focused on understanding the basis of their mechanism of substrate selectivity, both regarding binding and hydroxylation (5, 6).

Despite a highly conserved fold, P450s display a wide range of substrate specificities (7). Some cytochrome P450s show broad substrate and hydroxylation specificity and generally act as xenobiotic metabolizing enzymes, reacting with over 75% of pharmaceutical products on the market (8–10). On the other hand, other P450s, mostly involved in biosynthetic pathways, perform highly regio- and stereospecific hydroxylations.

The P450 from *Saccharopolyspora erythraea* CYP113A1, commonly called EryK, catalyzes one of the final steps of erythromycin A biosynthesis (Fig. 1). The initial steps of this biosynthetic pathway are performed by a polyketide synthase that carries out the condensation and stereospecific reduction of propionate with six molecules of methylmalonyl-CoA, producing the macrolactone 6-deoxyerythronolide B (11). EryK acts as a hydroxylase on the C-12 of the macrolactone ring of the metabolic intermediate erythromycin D (ErD).[5] This catalytic step follows the initial C-6 hydroxylation, performed by the P450 EryF, and the insertion of two deoxysugar units on the fifth and third positions of 6-deoxyerythronolide B, performed by glycosyl transferases EryBV and EryCIII, respectively. The biosynthetic pathway is then completed by a methyl transferase, EryG, which transfers a methyl moiety on the mycarosyl sugar (12, 13). EryG may also competitively act on ErD yielding a shunt metabolite, erythromycin B (ErB), which is an unsuitable substrate for further conversion by EryK to erythromycin A (14). This gives rise to significant shunt product accumulation during commercial fermentation of erythromycin A.

Here we report a structural and biophysical characterization of recombinant EryK. We obtained three different crystal structures, two in the ligand-free form and one bound to ErD. On the

* The work was supported by Italian MIUR FIRB2003 Grants RBLA03B3KC_004 and CNR RSTL2007-856.

[S] The on-line version of this article (available at http://www.jbc.org) contains supplemental Figs. S1–S5, Movies S1–S4, and Tables S1 and S2.

The atomic coordinates and structure factors (codes 2WIO, 2JJN, and 2JJO) have been deposited in the Protein Data Bank, Research Collaboratory for Structural Bioinformatics, Rutgers University, New Brunswick, NJ (http://www.rcsb.org/).

[1] Both authors contributed equally to this work.

[2] Present address: CNRS, Universités Aix-Marseille I et II, Case 932, Campus de Luminy, 13009 Marseille, Cedex 09, France.

[3] To whom correspondence may be addressed: Institute of Molecular Biology and Pathology, CNR, c/o Dept. of Biochemical Sciences, P.le Aldo Moro 5, 00185 Rome, Italy. Tel.: 3906-4991-0548; Fax: 3906-4440-062; E-mail: Stefano.gianni@uniroma1.it.

[4] To whom correspondence may be addressed. Tel.: 3906-4991-0548; Fax: 3906-4440-062; E-mail: beatrice.vallone@uniroma1.it.

[5] The abbreviations used are: ErD, erythromycin D; ErA, erythromycin A; ErB, erythromycin B; SRS, substrate recognition sites; BisTris, 2-[bis(2-hydroxyethyl)amino]-2-(hydroxymethyl)propane-1,3-diol; PDB, Protein Data Bank.

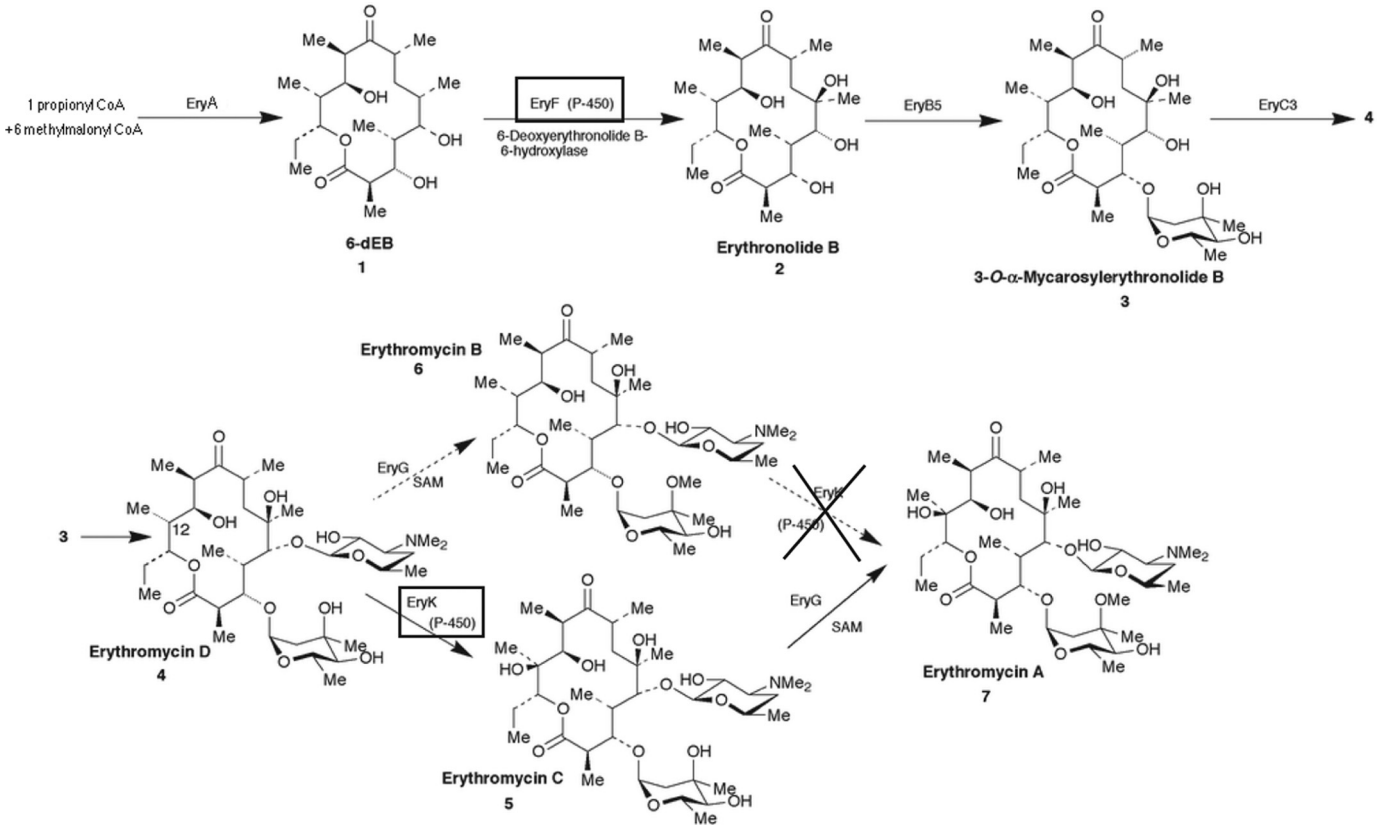

FIGURE 1. **Pathway of erythromycin A biosynthesis.** The reaction leading to the shunt product of ErB is indicated by the *dashed arrow*.

basis of these structures we propose a mechanism for substrate recognition and regioselectivity and we highlight the conformational changes involved in substrate binding to EryK. Furthermore, we show that the ligand-free structure of EryK may be shifted from an open to a closed state by increasing ionic strength conditions. In an effort to support these observations, we present an extensive characterization of the binding kinetics of EryK to ErD, using both single and double mixing time-resolved stopped-flow experiments. The significance of our results, in the context of previous characterization of the structure and function of P450s, will be also discussed.

MATERIALS AND METHODS

Sample Preparation and X-ray Data Collection—Recombinant His-tagged EryK was overexpressed in the BL21 STAR™ (DE3) *Escherichia coli* strain (Invitrogen) and purified as described previously (15). Purified EryK was concentrated and stored at 193 K. To assess its oligomerization state, EryK was subjected to ultracentrifugation in a Beckman Optima XL-1 instrument equipped with absorbance optics. Protein samples, measured at a concentration of 15 μM in the presence of 50 mM Tris·HCl, pH 7.5, at 298 K, were found to be monomeric (supplemental Fig. S1).

Three crystal forms of EryK were obtained in different crystallization conditions: with His tag (His_6-EryK) in low salt conditions, without tag (EryK) in high salt, and in complex with its substrate erythromycin D (ErD-EryK) (Table 1). All crystallization protocols were carried out at 294 K by vapor diffusion and ErD was introduced by co-crystallization. Diffraction data were collected at 100 K at the ESRF synchrotron (Grenoble, France) beamlines ID14-3 using a *mar*CCD detector, and ID14-2 using a ADSC Q4R detector. Data were integrated and scaled using the HKL suite (16), except for His_6-EryK data, which were processed with MOSFLM (17) and scaled with SCALA in the CCP4 suite (18). A summary is shown in Table 1.

Structure Determination and Refinement—In all cases molecular replacement was carried out to determine the initial crystallographic phases using the program MolRep (19) from the CCP4 suite (18). The ligand-free form of His_6-EryK was determined using EryF coordinates (20) (33.9% sequence identity, supplemental Fig. S2) as a search model (PDB code 1OXA). EryK was similarly determined by molecular replacement with His_6-EryK coordinates as a search model. EryK coordinates were used to solve the structure of ErD-EryK. Initial atomic models were subjected to iterative rounds of building and refinement. Refinement was carried out with Refmac5 (21) in CCP4, followed by model building and manual readjustment performed in QUANTA (Accelrys Inc.). Solvent molecules were added into the $F_o - F_c$ density map, contoured at 3σ, with the X-SOLVATE tool of QUANTA. Secondary structure assignment was performed using the Kabsch and Sander algorithm and geometrical quality of final models was assessed using PROCHECK (22). The first 14 to 18 N-terminal residues, depending on the crystal form, are missing in all models due to insufficient electron density in this region. Final statistics are shown in Table 1. All figures were produced with PyMOL.

TABLE 1

Data collections and refinements statistics

Highest-resolution shell is shown in parentheses.

	Protein name, PDB ID		
	Open EryK, PDB 2WIO	**Closed EryK, PDB 2JJN**	**ErD-EryK, PDB 2JJO**
Crystallization conditions	25% PEG 3350, 0.2 M NaCl, 0.1 M Tris-HCl, pH 8.0	2.0 M $(NH_4)_2SO_4$, 0.1 M BisTris, pH 6.5	25% PEG 3350, 0.2 M CH_3COONH_4, 0.1 M Tris-HCl, pH 8.5
Data collection			
Space group	$P2_12_12_1$	$P2_1$	$P2_1$
Cell dimensions (Å)	a = 37.93, b = 57.34, c = 179.56	a = 53.46, b = 68.00, c = 57.41, β = 101.05°	a = 57.84, b = 36.53, c = 96.00, β = 93.92°
Resolution (Å)	2.00 (2.01-1.91)	1.60 (1.66-1.60)	2.00 (2.15-2.00)
Completeness (%)	82.2 (85.9)	99.2 (97.9)	91.5 (80.4)
Redundancy	4.8 (4.7)	3.1 (2.6)	4.0 (3.1)
R_{merge} [a] (%)	19.3 (43.8)	3.9 (18.9)	5.9 (24.5)
$I/\sigma(I)$	10.9 (3.1)	19.9 (19.1)	13.0 (10.9)
No. reflections	22,459	53,461	25,564
B Wilson (Å^2)	19.7	16.1	19.5
Refinement			
Resolution (Å)	89.9-2.00	56.3-1.60	95.8-2.00
No. of atoms			
Protein/amino acid range	3096/19-411	3269/17-411	3096/19-411
Heme/ligand	43	43	43/49
Water/sulfate	309	546/25	335
R_{cryst}/R_{free} [b] (%)	18.3/23.2	16.1/19.8	16.9/23.6
Mean B-factors (Å^2)			
Protein	25.1	21.0	22.9
Heme	16.8	11.8	13.0
Substrate			15.7
Water/ion	33.3	32.0/31.1	26.5
Root mean square deviations			
Bond (Å)	0.014	0.016	0.013
Angles (°)	1.543	1.665	1.624
Ramachandran (%)			
Most favored/allowed/generous/disallowed	89.3/10.7/0/0	91.2/18.2/0.3/0.3	90.8/8.0/0.9/0.3

[a] $R_{merge} = \Sigma_i\Sigma_j|I_{i,j} - \langle I_j\rangle|/\Sigma_i\Sigma_j I_{i,j}$, where i runs over multiple observations of the same intensity, and j runs over all crystallographically unique intensities.
[b] $R_{work} = \Sigma||F_{obs}| - |Fcalc||/\Sigma|F_{obs}|$, where $|F_{obs}| > 0$. R_{free} is based on 5% of the data randomly selected and is not used in the refinement.

Root mean square deviation and sequence identity among the structures of EryK, PikC, and EryF were determined using CE (23). Sequence numbering refers to EryK (SwissProt accession A4FNo_SACEN; NCBI accession YP_001102980); secondary structure elements are named following P450 convention.

Spectral Binding Titrations—Because catalysis would require the presence of external reducing agents and EryK was purified in its oxidized form, addition of ErD results in monitoring only the binding reaction (12). Thus, all the experiments reported in this work refer to the binding reaction of EryK to ErD, in the absence of catalysis. Binding affinities of ErD to EryK in different ionic strength conditions were determined (at 298 K) by titrating 2 μM enzyme with the ligand, ErD, in a total volume of 800 μl of 50 mM Tris·HCl buffer, pH 7.5, with and without 2 M NaCl. Ligand concentration covered a suitable range from 0 to 300 μM. UV visible spectra (190–820 nm) were recorded after each addition and the absorbance intensities at 420 and 390 nm were plotted against the logarithm of the added ligand concentrations (data not shown). From each of the substrate-bound spectra were subtracted the appropriate blank.

The dissociation constant (K_D) was estimated using the Kaleidagraph software package. A nonlinear regression analysis was applied using hyperbolic equation $\Delta AU_{obs} = \Delta AU_{max}[L]/(K_D + [L])$, where ΔAU_{obs} is the absorbance difference, ΔAU_{max} is the maximum absorbance difference extrapolated to infinite ligand concentration, and [L] is the ligand analytical concentration. Data were also globally fitted with the program Prism (Graphpad).

Ligand Binding Kinetics—The time evolution of the EryK-ErD interaction was followed by monitoring the change in absorbance at 390 nm on a stopped-flow apparatus. Measurements were performed on a SX18-MV stopped-flow instrument (Applied Photophysics, Leatherhead, UK) using both symmetric and asymmetric (1:10) mixing. In the symmetric mixing mode, EryK, at a final constant concentration of 7.5 μM, was mixed with ErD diluted to the desired final concentration, varying in a range from 9 to 150 μM. The traces were recorded in 50 mM Tris·HCl, pH 7.5, at 288 K, both in the absence and presence of 2 M NaCl. In the asymmetric mixing mode, varying the NaCl concentration in a range from 0 to 3.6 M, the kinetic traces of the interaction between EryK (final constant concentration of 5.5 μM) and ErD (final constant concentration of 100 μM) were recorded at 288 K in 50 mM Tris·HCl, pH 7.5. Kinetic traces were extracted from the acquired spectra (recorded as average of at least three experiments) and analyzed using the Kaleidagraph software package.

Double Jump Measurements—To characterize the pre-equilibrium stage of the open and closed conformations of EryK, we performed double mixing measurements carried out in 50 mM Tris·HCl, pH 7.5, by using an Applied Photophysics SX18-MV stopped-flow instrument at 288 K. EryK (13.5 μM) was incubated in 2 M NaCl for different delay times and then symmetrically mixed with ErD at a final concentration of 100 μM, in 50 mM Tris·HCl, pH 7.5, with 2 M NaCl. The observed amplitudes, reflecting the fraction of molecules populating the open and closed conformations, were plotted as a function of delay times and fitted to a single exponential decay.

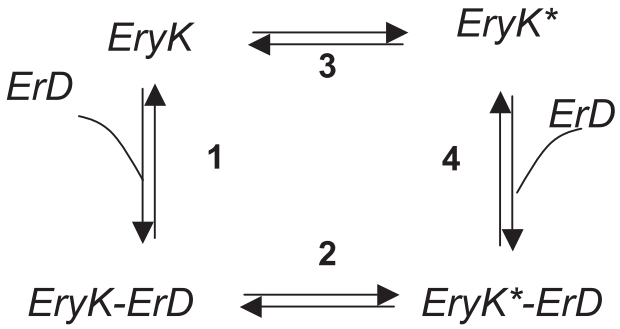

SCHEME 1

Kinetic Models—Classically, complex kinetics for a monomeric protein, as EryK, undergoing a ligand-induced conformational change, is described by the Scheme 1. A binding event progressing through pathways **1** and **2** is representative of an *induced fit* model, whereby ligand binding is postulated to induce a conformational change (24), which may be transmitted to neighboring residues as shown in Scheme 2.

$$\mathrm{EryK} + \mathrm{ErD} \underset{k_{-1}}{\overset{k_1}{\rightleftharpoons}} \mathrm{EryK-ErD} \underset{k_{-2}}{\overset{k_2}{\rightleftharpoons}} \mathrm{EryK^*-ErD}$$

SCHEME 2

Under such conditions, observations of biphasic kinetics arise from the accumulation of the EryK-ErD reaction intermediate. When and if the fast phase is $\lambda_1 \gg \lambda_2$, the fast phase λ_1 is due to the initial encounter between the EryK and ErD molecules, with an observed rate constant shown in Equation 1.

$$\lambda_1 = k_1[\mathrm{ErD}] + k_{-1} \qquad \text{(Eq. 1)}$$

Furthermore, the slow phase λ_2 is then expected to increase hyperbolically with increasing ErD concentration as shown in Equation 2.

$$\lambda_2 = k_{-2} + k_2\frac{[\mathrm{ErD}]}{K'_D + [\mathrm{ErD}]} \qquad \text{(Eq. 2)}$$

where

$$K'_D = \frac{k_{-1}}{k_1} \qquad \text{(Eq. 3)}$$

In this case, λ_2 is expected to equal k_{-2} at [ErD] = 0 and (k_{-2} + k_2) at [ErD] $\rightarrow \infty$.

Alternatively, a binding event progressing through pathways **3** and **4** assumes that two alternative conformations are in pre-equilibrium in the absence of the ligand, formally similar to a concerted or conformational selection model (25). Accordingly, complex kinetics may arise from a heterogeneous conformational ensemble of EryK, which may populate, in the absence of ligand, experimentally detectable populations of both EryK and EryK*.

$$\mathrm{EryK} \underset{k_{-1}}{\overset{k_1}{\rightleftharpoons}} \mathrm{EryK^*} + \mathrm{ErD} \underset{k_{-2}}{\overset{k_2}{\rightleftharpoons}} \mathrm{EryK^*-ErD}$$

SCHEME 3

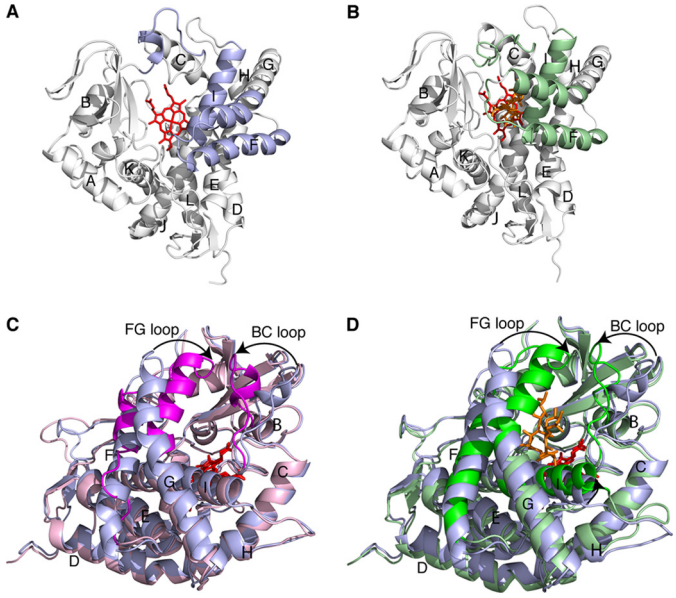

FIGURE 2. **Structures of EryK.** *A*, the structure of the open EryK is shown, the elements that move upon substrate binding are highlighted in *blue*. *B*, substrate bound EryK, the elements that close on the active site are given in *green*. *C*, superposition of closed (*pink* and *magenta*) and open ligand-free structures of EryK. *D*, superposition of the open (*blue*) and substrate-bound (*light* and *dark green*) structures of EryK. The *arrows* point toward the FG and BC loops, which undergo the most pronounced displacement. Heme groups are in *red*, ErD in *orange*, and *capital letters* indicate the helices according P450 nomenclature. *Panels A* and *B* show EryK in the standard P450 orientation, whereas *panels C* and *D* utilize an orientation that allows clear visualization of the structure transitions.

Under such conditions, and if $k_{-2} \gg (k_1 + k_{-1})$, the fast phase would arise from an initial population of monomers in the EryK* conformation and would occur with a rate constant as described in Equation 4.

$$\lambda_1 = k_2[\mathrm{ErD}] + k_{-2} \qquad \text{(Eq. 4)}$$

On the other hand, the slow phase λ_2 is expected to decrease hyperbolically with increasing ErD concentration as shown in Equation 5.

$$\lambda_2 = k_1 + k_{-1}\frac{K'_D}{K'_D + [\mathrm{ErD}]} \qquad \text{(Eq. 5)}$$

where

$$K'_D = \frac{k_{-2}}{k_2} \qquad \text{(Eq. 6)}$$

In this case, λ_2 is expected to approach (k_{-1} + k_1) at [ErD] = 0 and k_1 at [ErD] $\rightarrow \infty$.

RESULTS

Overall Structure

EryK displays the typical topology of previously characterized P450s (Fig. 2). This enzyme shows the highest sequence identity with EryF (33.9%), which is involved in the same biosynthetic pathway (see supplemental Fig. S2). The conserved protein core is formed by a four-helix bundle, three parallel helices (D, L, and I) and an antiparallel one (E). The prosthetic heme group is located between the distal helix I and

the proximal helix L and it is bound to Cys[353], the highly conserved fifth ligand of the heme iron. Despite a conserved overall structure, P450s display a wide range of substrate specificities (1). At a structural level, P450 substrate recognition and binding is assured by six so called "substrate recognition sites" (SRS) that line the active site (26). Although the definition of SRS becomes obsolete once the structure has been determined and precise protein-substrate contacts have been revealed, we will use in this section this nomenclature to define the amino acid topology because in EryK the elements that contact the substrate correspond to these SRS. These regions are: SRS1, formed either by the BC loop (as in EryK) or the B′ helix (as in EryF); SRS2 formed by the C-terminal part of helix F; SRS3 formed by the N-terminal part of helix G; SRS4 formed by the central part of the distal helix I; SRS5 formed by the loop at the C-terminal end of helix K; SRS6 formed by the β-hairpin β4 (supplemental Fig. S2). Some SRSs may rearrange upon substrate binding, formally following an induced fit scenario (4).

The superposition of the crystal structures of the two ligand-free forms of EryK (Fig. 2*C*), obtained at low and high salt, reveals that there are two different conformations for this protein in the unbound state, involving, among others, a movement of the BC loop of about 11 Å. Furthermore, helix G kinks at the level of Pro[192], causing its N-terminal part to shift about 10 Å toward the BC loop. Interestingly, Pro[192] is not conserved in homologous P450. The movement of helix G also pulls the FG loop and helix F, causing the latter to unwind almost completely (Figs. 2*C* and 3*A*, and supplemental Movie 1). This reorganization, observed in the EryK structure at high ionic strength, closes the access channel for the active site of the molecule.

Although the last two C-terminal turns of helix F keep parallel to the moving part of helix G, its N-terminal part (Asp[158]–Asp[164]) adopts a coil conformation upon active site closing. As shown in detail in Fig. 3*C*, the coil conformation of helix F causes the loss of a H-bond between His[243] and Ser[166] and contact between Trp[165] and Pro[192] that connect helix I to helix G through helix F in an open ligand-free EryK structure obtained at low ionic strength. Moreover, Trp[165] rotates and docks in a new position pointing toward helix I and interacts with His[243] (supplemental Movie 2). In summary, these rearrangements result in a marked reduction of the exposure of the heme distal site that identifies two different conformations to which we will refer to as "open" and "closed" depending on the position of helices F and G and the BC loop. Importantly, an open/closed transition has been previously observed in other P450s, as in the case of the *Bacillus megaterium* flavocytochrome P450 BM3 (CYP102) (27, 28) and PikC (CYP107L1), the *Streptomyces venezuelae* P450 involved in C-12 hydroxylation in the pikromycin biosynthetic pathway (29).

ErD-EryK Structure

Determinants of Substrate Selectivity—We co-crystallized EryK in a complex with ErD. The well defined electron density of the substrate was unambiguously positioned in the active site (Fig. 3*B*). The cavity hosting the substrate involves essentially two regions: a fixed one, formed by the loop at the helix K

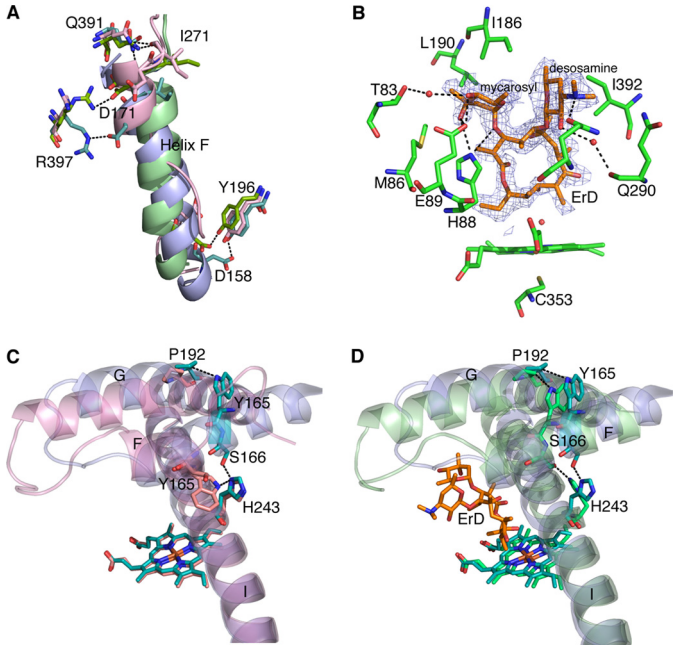

FIGURE 3. **Substrate recognition and locking within the active site of EryK.** *A*, a close up of the helix F network in superposed open EryK (blue), ligand-free closed EryK (*pink*), and ErD-EryK (*green*). Superposition was based on secondary structure motifs as implemented in COOT (48). *B*, view of contacts between the EryK and its substrate ErD. The electron density omit map ($2F_o - F_c$) is contoured at 1.0σ around ErD. *C*, the HSWP network is shown for ligand-free closed EryK (*pink*), superposed to open EryK (*blue*). *D*, the HSWP network is shown for ErD-EryK (*green*), superposed to open EryK (*blue*). Heme groups, substrate (*orange*), and side chains are in *sticks*. *Dashed lines* indicate H-bonds and close contacts, the actual distances are given in supplemental Tables S1 and S2.

C-terminal, the β-hairpins β4 and β1 (Asp[46]–Gly[49]), and a mobile one, formed by the BC loop and the F and G helices.

A central feature of ErD recognition involves anchoring of the two sugar substituents, a desosamine on C-5 and a mycarosyl group on C-3 of the macrolactone ring (supplemental Table S1 and Fig. 3*B*). Desosamine interacts mainly with the loop at the helix K C-terminal, by two H-bonds with Gln[290] and Gln[292]; moreover, Ile[392] in the β-hairpin β4 ensures the sugar clamping by van der Waals contacts. It is worth emphasizing that this is the only amino acid close to the forbidden conformation in the Ramachandran plot for the refined ErD-EryK structure, suggesting a critical structural role (30, 31). All these interactions would be absent for a ligand lacking the desosamine sugar as in the case of the biosynthetic intermediate MycEB (see Fig. 1). Mycarose interacts with the mobile part of the channel establishing four crossed H-bonds with His[88] and Glu[89] on BC loop (Fig. 3*B*). Its position is also restricted by van der Waals interactions with the FG loop, which closes down on top of it. Substrate binding can therefore be described as landing on the fixed region followed by closure of two "arms" consisting of the BC loop and the F and G helices.

The selectivity for ErD against ErB is clearly explained by this structure. Indeed, methylation of 3′-OH would interfere with the complete closure of the arms to embrace the substrate, caused by clashes with Met[86], His[88], and Glu[89] in the BC loop.

The macrolactone ring of ErD establishes hydrophobic interactions with residues on helix I, helix K on the C-terminal, and β-hairpin β4 (Table S1). Ile[244] and Thr[245] on helix I lie in the

active site, and the amino acids in these topological positions are believed to be involved in catalysis, playing a role in stabilization and proton delivery to the iron-bound dioxygen species (32). Altogether packing the macrolactone ring against the heme and SRS4 is very tight, explaining why limited hydroxylation at C-12 was observed when bulky substituents were introduced in C-13 (33, 34) and also why there is no flexibility allowed for substrate hydroxylation sites, as observed for PikC (29), where empty pockets in the binding site are present.

In ErD-EryK, the target of hydroxylation C-12 of the macrolactone ring is positioned 5.3 Å from the heme iron. Similar distances between the hydroxylation site and the iron have been reported for other P450s, such as EryF (Fe-C6 4.8 Å) and $P450_{cam}$ (Fe-C5 4.2 Å) (35). The water molecule bound to the oxidized heme iron in the ligand-free structure of EryK disappears and a new one (Wat^{102}) is found at 2.7 Å from the metal, which is H-bonded to the substrate 11-OH group. This water occupies a position that almost coincides with the O-2 atom of dioxygen bound to $P450_{cam}$. Two more water molecules are found in the vicinity of Thr^{245}, Wat^{4} and Wat^{38}, which in $P450_{cam}$ appear upon dioxygen binding (36). Moreover, Wat^{27} is also positioned as in $P450_{cam}$, hydrogen bonded to conserved Asp_{362}.

Therefore, taking into account the carbonyl atom of Gly^{242}, in ErD-EryK we find a water molecule chain that leads from the active site to the bulk. This network corresponds closely to that observed in the oxygen-bound form of $P450_{cam}$, with Wat^{102} mimicking the bound dioxygen (supplemental Fig. S3). From this work we cannot determine the mechanism of EryK catalysis, but given the conservation of water molecules in the active site and Thr^{241}, we may infer that the general catalytic mechanism proposed for bacterial P450 is conserved.

Closing and Locking Mechanism—Structural rearrangements due to substrate binding occur in the most dynamic regions of EryK (F and G helices and BC loop). Movements of these elements are not hindered from crystal contacts in open, closed, and closed-bound EryK. The ErD-EryK structure resembles the closed ligand-free form (Fig. 2, *B* and *D*), but new interactions are found that work as a molecular device that switches upon substrate binding. The movement of the BC loop in ErD-EryK is less pronounced than in the closed ligand-free form, because interactions with the mycarose hinder its full transition. Moreover, helices F and G move less on top of the substrate channel (9 Å displacement instead of 11 Å); helix G kinks at the level of Pro^{192} and, together with the FG loop, adopts a conformation similar to the closed ligand-free structure (Cα differences "ligand-free closed"/ErD-EryK ~ 1.5 Å). Helix F in the ErD-EryK structure follows the movement of helix G, being lifted about one turn (3.7 Å) and tilted by 13°. This helix is not unwound on its N-terminal side, whereas in the ligand-free closed structure it loses the α helix geometry almost completely (Figs. 2*B* and 3*A*, and supplemental Movie 3). Therefore, in the open and substrate-bound structures, helix F is present and held by H-bonds with β-hairpin β4 and helix G, whereas such interactions are absent in the ligand-free closed structure where this helix is only two turns long (Fig. 3*A* and supplemental Table S2).

Helix I is slightly distorted in its central part, between Ile^{239} and Thr^{245}, in both ligand-free EryK structures, whereas in ErD-EryK it shows pronounced bending due to extensive interactions of the macrolactone ring with side chains of residues in its middle segment (Ala^{237}, Leu^{240}, Ala^{241}, Ile^{244}, and Thr^{245}). This bending induces flipping and reorientation of His^{243} on helix I (supplemental Movie 4) that can establish a H-bond with Ser^{166}, located on helix F. This interaction, lost when EryK closes without ErD, allows helix F to not unwind and to shift following helix G kinking, thus moving as a rigid unit. As a consequence of helix F repositioning, Trp^{165} exerts pressure on Pro^{192} on helix G. Upon this pressure Pro^{192}, the hinge that allows G helix kinking is locked, preventing reopening (Fig. 3*D*).

Importantly, whereas helix G kinking and repositioning of mobile elements can take place also in the absence of ErD, this network of interactions (called HSWP network after His^{243}, Ser^{166}, Trp^{165}, and Pro^{192}) is present only if the substrate is clamped in the active site. The HSWP network is the connection that couples helix G kinking to helix I bending through helix F, and acts as a connecting rod, when substrate is bound, whereas it unwinds in the ligand-free closed structure. The HSWP network involving the same residues was also found in open EryK, but with a geometry that does not induce helix kinking. Therefore, the presence of the correct substrate, ErD, is sensed at two levels: bending of helix I to recognize the presence of the macrolide ring to be hydroxylated thus locking G helix kinking, and recognition of the mycarosyl sugar by the BC loop that specifically interacts with its 3′-OH.

Very recently the structure of a P450 (CYP199A2) from the highly metabolically versatile *Rhodopseudomonas palustris* (37, 38) was reported, showing a structure with a kinked G helix at a proline corresponding to Pro^{192} of EryK, and no B′ helix. This peculiar conformation of G helix is therefore adopted in more than one P450, although it is difficult to conclude whether it is coming from convergent evolution or gene transfer. We hypothesize that the presence of proline in a position topologically equivalent to Pro^{192} in EryK and Pro^{204} in CYP199A2 is a signature indicating the presence of a kink in the G helix to compensate for the absence of the B′ helix.

Are the Two Ligand-free Structures a Crystallographic Artifact? The Kinetics of Binding EryK to ErD

Crystallographic studies, reported above, reveal that it is possible to obtain two different and stable conformations of ligand-free EryK under conditions that differ mainly in ionic strength of the solution. We therefore hypothesized that free EryK in solution could exist in a heterogeneous pool of stable conformations that have different abilities to bind the ligand and are selectively stabilized by ionic strength conditions. To probe the existence of different EryK conformers, we compared static UV visible spectra and circular dichroism spectra of free EryK in the presence and absence of high ionic strength buffer conditions (data not shown). Contrary to previous work on other P450 (39, 40), we observed that the absorption spectrum of EryK is insensitive to the ionic strength of the solution. These observations suggest that either EryK can accumulate only one discrete conformation under the conditions investigated in this study or no significant spectroscopic changes may be associated with the

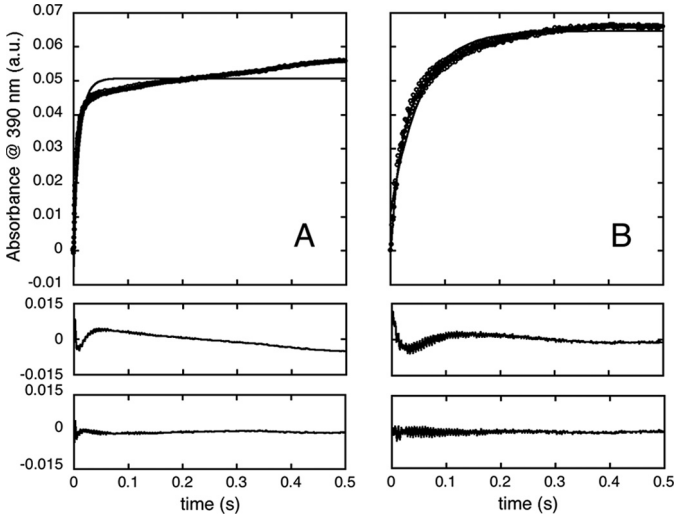

FIGURE 4. **Binding kinetics of EryK to ErD.** The *traces* reported were obtained at 90 μM ErD and 7.5 μM EryK in the absence (*panel A*) and presence (*panel B*) of 2 M NaCl. Traces reported are the averages of three independent acquisitions. The residuals to a single (*top*) and double (*bottom*) exponential fit are reported *below* each trace. *Thin lines* are the fit to a single exponential decay.

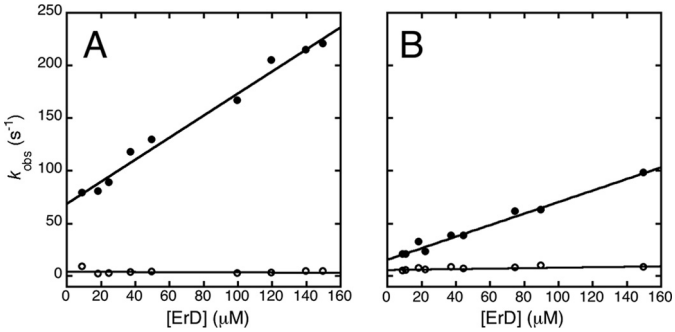

FIGURE 5. **Binding kinetics of EryK to ErD.** Observed rate constants are plotted as a function of [ErD]. The rate constants for the fast phase (*filled circles*) increase linearly with increasing [ErD], whereas the rate constants for the slow phase (*empty circles*) are essentially independent on [ErD]. *Panels A* and *B* refer to data recorded in the absence and presence of 2 M NaCl, respectively.

conformational change described above. In an effort to validate the existence of the two alternative conformations, we performed a complete characterization of the binding properties of EryK at high and low ionic strength conditions.

Upon binding to ErD, EryK exhibits the spectral changes classically observed for previously characterized cytochrome P450s (4, 6, 8), *i.e.* a shift of the Soret peak from 420 to 390 nm. These spectral changes have been previously reported (12). Equilibrium binding experiments measured in the presence and absence of 2 M NaCl display a simple hyperbolic transition yielding an apparent K_D of 3.5 ± 0.1 and 1.0 ± 0.1 μM in the absence and presence of 2 M NaCl, respectively (data not shown).

We studied the binding kinetics of EryK to ErD by following the absorbance of the heme iron at 390 nm. Experiments were performed under pseudo first-order conditions by challenging EryK, at a constant concentration of 7.5 μM, with increasing concentrations of ErD. Two typical kinetic traces recorded in the presence and absence of 2 M NaCl are reported in Fig. 4. At all monitored conditions, observed kinetics displayed a systematic deviation from a single exponential function and were fitted satisfactorily to a double exponential equation, suggesting that the binding of ErD to EryK occurs via at least two steps.

Inspection of Fig. 4 clearly reveals that addition of 2 M salt affects the relative amplitudes of the observed phases. The fast phase changes from about 90% of the total signal change in the absence of salt to about 60% in its presence. In an effort to further test the effect of the NaCl concentration on the relative amplitudes of the observed phases, we performed kinetic experiments at constant EryK and ErD concentrations (5.5 and 100 μM, respectively) and at different salt concentrations (supplemental Fig. S4). Interestingly, the relative amplitude of the slow phase clearly increases at higher salt concentrations.

A plot of the observed rate constants for the two phases as a function of ligand concentration are reported in Fig. 5. Overall, whereas the rate constants for the fast phase appear to increase linearly with increasing ligand concentration, the rate constants for the slow phase are essentially independent of [ErD]. Notably, a similar behavior was observed in the presence of 2 M NaCl. The calculated rate constants from analysis of the fast phases were: $k_{on} = (1.05 \pm 0.06) \times 10^6\ M^{-1}\ s^{-1}$ and $k_{off} = 70 \pm 5\ s^{-1}$ in the absence of salt, and $k_{on} = (5.5 \pm 0.3) \times 10^5\ M^{-1}\ s^{-1}$ and $k_{off} = 16 \pm 2\ s^{-1}$ in the presence of 2 M NaCl. The two experiments revealed the presence of a slow phase, λ_2, independent on ErD concentration, of about $4 \pm 0.4\ s^{-1}$ and $1.3 \pm 0.1\ s^{-1}$ in the absence and presence of salt, respectively.

As discussed under "Materials and Methods," analysis of λ_2 on substrate concentration should in theory be of diagnostic value to understand which of the two possible mechanisms best describes the experimental data (41, 42), *i.e.* a mechanism involving a pre-existing conformational heterogeneity of EryK or a mechanism involving an induced fit scenario. However, as described below, in the case of the interaction between EryK and ErD we could not obtain any clear dependence of λ_2 on [ErD], the observed rate constant being essentially independent on [ErD] both in the presence and absence of NaCl. This effect may be due to either (i) a low value of K_D', which would imply λ_2 to reach a constant value at relatively low [ErD] or (ii) a low value of k_2 or k_{-1} in Schemes 2 or 3, respectively, which would result in a λ_2 nearly independent on [ErD] (see Equations 2 and 5 under "Materials and Methods").

Comparison between the two models outlined above reveals that, whereas in the case of the induced fit scenario (Scheme 2) biphasic kinetics arise from accumulation of a genuine reaction intermediate (the EryK-ErD complex), in the case of the conformational selection model (Scheme 3), complex time courses may only occur when the EryK and EryK* states display a similar stability, *i.e.* they are both populated prior to encountering the ligand. Hence, to distinguish between the induced fit and conformational selection scenarios, we performed a double jump stopped-flow mixing experiment. Analysis of the NaCl dependence of observed kinetics reveals that the amplitude of the slow phase is increased with increasing ionic strength (supplemental Fig. S4). Following Scheme 3, it may be postulated that high NaCl concentrations shift the equilibrium toward the EryK conformer. It may be noted that the crystal structure of EryK under low and high ionic strength conditions reveals the presence of two different conformers, namely an open and a

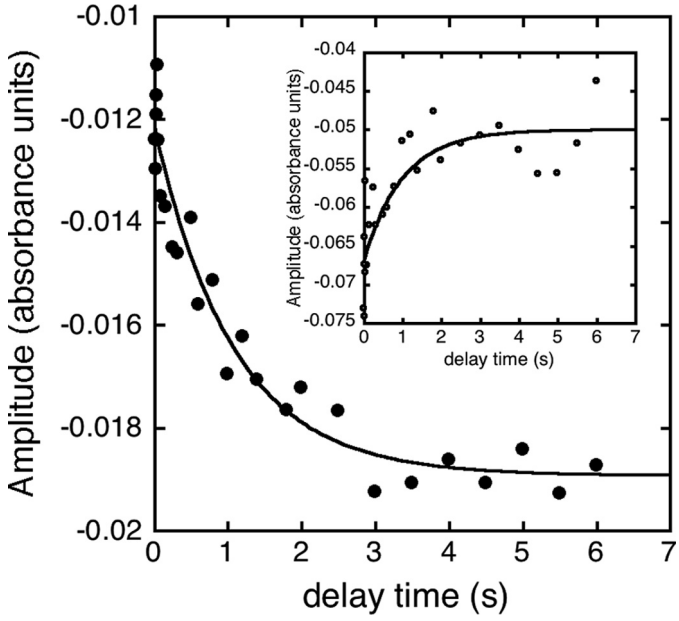

FIGURE 6. **Double jump mixing experiments monitoring the binding of EryK to ErD.** The amplitudes for the two phases are reported as a function of the delay time between the first and second mix (see text for details regarding the experimental setup). The amplitudes obtained for the slow phase (*filled circles*) and for the fast phase (shown in the *inset*) were globally fitted to a single exponential function, yielding a value of $k_{obs} = 1.8 \pm 0.1\ s^{-1}$.

closed state. Thus, the double jump experimental setup was designed with the specific aim of altering the relative populations of the two conformers before mixing them with the substrate. In particular, the protein was first mixed with a constant concentration of 2 M NaCl (first mix); after a controlled delay time, the reaction mixture was challenged with ErD at a constant concentration of 50 μM (second mix). At all different delay times, the observed time courses were fitted to a double exponential function, which returned similar rate constants for both phases. Importantly, the observed amplitudes of the two phases display a single exponential dependence on the delay times between the first and the second mix, yielding an apparent rate constant of $1.8 \pm 0.1\ s^{-1}$ (Fig. 6). Inspection of Fig. 6 clearly reveals that although the amplitude of the fast phase decreases with increasing delay times, the slow phase increases. This behavior is inconsistent with an induced fit model (Scheme 2). In fact, because this model postulates the existence of only one conformer prior to encountering of the ligand, it would imply that the relative amplitudes of the two phases are independent of the delay times. On the other hand, by assuming a conformational selection model (Scheme 3), data presented in Fig. 6 allow direct measurement of the observed rate constant for structural rearrangement (*i.e.* $k_1 + k_{-1} = 1.8 \pm 0.1\ s^{-1}$ at 2 M NaCl). Because we know the k_1 from the experiment shown in Fig. 5, the microscopic rate constant, k_{-1}, can then be calculated as $0.5\ s^{-1}$. The fractions of open and closed conformations from rate constants (0.7 and 0.3, respectively) agree well with those from kinetic amplitudes (supplemental Fig. S5).

We conclude that the biphasic kinetics of binding EryK to ErD arises from a conformational selection mechanism, whereby the protein pre-exists in two alternative states, where only one binds the substrate. Addition of NaCl shifts the equilibrium toward the closed state, as mirrored by the increased relative amplitude of the slow kinetic phase. Double jump mixing experiments allow (i) to exclude a kinetic mechanism involving an induced fit scenario and (ii) to monitor directly the observed rate constant of the conformational change reaction ($k_1 + k_{-1}$).

DISCUSSION

The structures of EryK highlight novel structural features, with respect to other related P450s, which are necessary to allow a complete and competent recognition and closure around the bulky substrate, a macrolactone ring carrying two sugar substituents. A relevant comparison can be carried out with respect to the structures of EryF bound to the macrolide 6-deoxyerythronolide B (20) and that of PikC, which binds a monoglycosylated macrolide, narbomycin (29). In EryF, elements B′ helix, BC loop, and FG loop close like a lid on the substrate; this is also the case for PikC, where the extra bulk, represented by a desosamine, is accommodated by shortening of the BC loop. The presence of a second sugar moiety as in ErD exceeds this plasticity. As a result, in EryK the role of helix B′ in closing the channel is taken by the N-terminal part of helix G, which contains a hinge (Pro^{192}) allowing a straight to kinked transition. With respect to EryF and PikC we also observed a longer FG loop, a rearrangement of helix F, and a reduction in size of the β hairpin, β4.

On the basis of the two structures determined in the absence of substrate, we propose that both open and closed conformations are populated in solution: low salt and high salt crystallization conditions are able to shift this equilibrium, inducing the crystallization of either of the two forms. Kinetic data confirm this hypothesis because double jump experiments reveal that complex binding arises from a pre-existing conformational heterogeneity of substrate-free EryK. It may be noted that at physiological salt conditions, the closed conformer accounts for only 10% of the molecules, suggesting that biologically relevant processes are likely to involve mostly the open conformation. Yet, defining the relative stabilities of the two conformers may be significant in at least two ways. First, previous work has described the binding reaction of P450s to their ligands with an induced fit model, essentially on the basis of the observation of multiple exponentials. Although this could well be true for many P450s, such as 3A4, our experimental work on EryK shows that biphasic kinetics may also arise from a pre-existing equilibrium of protein conformers. Second, a population of about 10% implies that the free energies of the open and closed conformations are similar. Thus, in theory, it would be possible to shift the equilibrium between the two conformers, for example, via site-directed mutagenesis or ligand binding. The description of the structure and energetics of the two conformations paves the way for future work in this direction.

It is of interest to comment on the magnitude of the kinetic constants for the binding of EryK to ErD, in comparison with crystallographic data. In fact, the rate constants obtained for the encounter of the open conformation to ErD, *i.e.* $(1.05 \pm 0.06) \times 10^6\ M^{-1}\ s^{-1}$ and $(5.5 \pm 0.3) \times 10^5\ M^{-1}\ s^{-1}$ in the absence and presence of salt, respectively, are somewhat lower than expected from a diffusion-controlled reaction (43). This

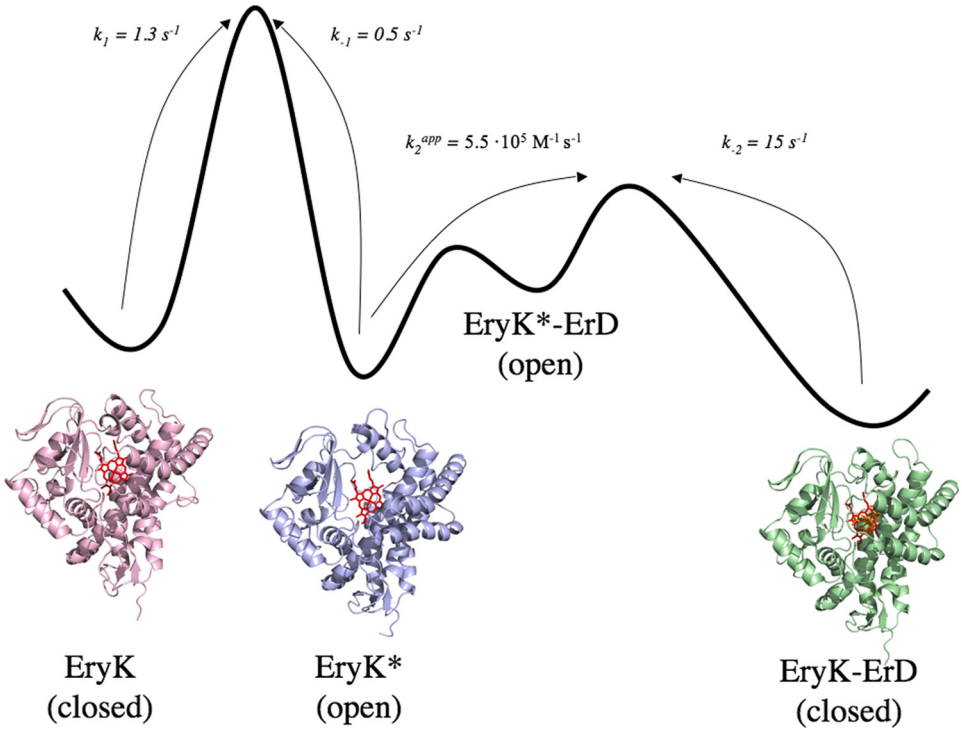

FIGURE 7. **Schematic energy diagram showing the binding reaction of EryK to ErD.** Representative structures of closed-free (*pink*), open-free (*blue*) EryK, and the ligand-bound ErD-EryK (*green*) are also shown. It should be noted that, given that observed kinetics is well fitted by a double exponential process under all investigated conditions, the existence of a late closure step may only be invoked indirectly from crystallographic work, as well as from the slow apparent second-order rate constant. The microscopic rate constants, obtained in the presence of 2 M NaCl, were calculated as reported below. As described in the text, we designed a double jump experiment with the specific aim of shifting the equilibrium between the open and closed states, prior the encountering the ligand. Hence, the amplitude dependence of the two phases as a function of the delay time (Fig. 6) directly reports on the kinetics of the first step in Schemes 3 and 4, the observed rate constant k_{obs} being equal to $(k_1 + k_{-1}) = 1.8 \pm 0.1\ s^{-1}$. On the other hand, by considering that the binding reaction between the open conformer of EryK and ErD occurs faster than the conformational change between the open and closed states of EryK, the rate constant for the slow phase λ_2 should tend to be k_1 at [ErD] $\rightarrow \infty$ (see Equation 5). Data in Fig. 5 clearly reveal that λ_2 is independent on [ErD], suggesting that the limiting value of k_1 is reached at relatively low [ErD] and equal to $1.3 \pm 0.1\ s^{-1}$. Based on these observations, we estimated a value of $k_{-1} = 0.5 \pm 0.1\ s^{-1}$. Importantly, a similar magnitude of k_1 and k_{-1} are consistent with the proposed heterogeneous conformation of EryK, the equilibrium constant of the first step being equal to k_1/k_{-1}.

observation suggests the presence of an additional step after recognition between open EryK and ErD, which may correspond to the interactions that lock the substrate in the active site (HSWP network).

It should be noted that the crystal structure of the final complex closely resembles the structure of the closed-free state. On the basis of these observations, we then conclude that a plausible mechanism describing the binding reaction of EryK to ErD would involve an additional step implying the locking of the enzyme, as formalized in Scheme 4,

$$\mathrm{EryK} \underset{k_{-1}}{\overset{k_1}{\rightleftharpoons}} \mathrm{EryK^*} + \mathrm{ErD} \underset{k_{-2}}{\overset{k_2}{\rightleftharpoons}} \mathrm{EryK^*} - \mathrm{ErD} \underset{k_{-3}}{\overset{k_3}{\rightleftharpoons}} \mathrm{EryK} - \mathrm{ErD}$$

SCHEME 4

where EryK and EryK* denote the closed and open conformers, respectively. Although the experimental work presented here allows inference directly in the presence of a pre-existing conformational heterogeneity of EryK (step 3 in Scheme 1), the existence of a late closure step may be invoked only indirectly from the crystallographic work, as well as from the observed slow apparent second-order rate constants. A quantitative analysis of crystallographic and kinetic data of the binding of EryK to ErD is summarized in the energy diagram in Fig. 7.

Substrate binding to P450s has been extensively studied and is still an area of major interest (5). However, despite many efforts, there are still more exceptions than rules when it comes to binding a substrate to different P450s and a unifying comprehensive mechanism is yet to be unveiled. One of the most extensively characterized cytochrome P450s is the human cytochrome P450 3A4. In particular, Guengerich and co-workers (44, 45) recently reported a comprehensive analysis of the binding kinetics of this enzyme to its specific ligands and inhibitors. Contrary to what we observed for EryK, it was concluded that multiphasic kinetics of P450 3A4 is a result of sequential events of binding as opposed to the existence of multiple enzyme populations in dynamic equilibrium. One of the key findings to support this hypothesis was based on the existence of a fast phase, which is silent in absorbance, but detectable with fluorescence, possibly as a result of binding multiple ligands to a peripheral site of the enzyme. Consistently with Scheme 3, EryK does not display this absorbance-silent phase, as monitored by fluorescence with ketoconazole.[6] Another possible model, which would account for the kinetic data presented in this work, is oligomerization of the enzyme (46). However, analytical ultracentrifugation profiles of EryK clearly show that the protein is monomeric at the concentrations investigated in this work (*i.e.* 5–15 μM).

In conclusion, we present a clear example of a monomeric P450, whose complex binding kinetics are dictated by the presence of a heterogeneous conformational ensemble between an open and a closed state. Future studies based on protein engineering will further clarify the molecular details of the recognition of EryK with its physiological substrate ErD and possibly allow the design of an enzyme that hydroxylates substrates containing a cladinose sugar. This may result in greater levels of the desired ErA and would represent an alternative method of achieving better ErA/ErB ratios to that recently achieved

[6] C. Savino, L. C. Montemiglio, S. Gianni, and B. Vallone, manuscript in preparation.

through up-regulation of EryK or by engineering a higher substrate specificity into the methyltransferase EryG (14, 47).

Acknowledgments—We thank Barrie Wilkinson and Rachel Lill (Biotica Technology) for the kind gift of erythromycin D. We gratefully thank Daniela Verzili and Carlotta Zamparelli (IBPM, CNR, and Department of Biochemical Sciences, Sapienza, Rome). We are grateful to synchrotrons ESRF (beamlines ID14-3 and ID14-2, Grenoble, France) and the European Community-Research Infrastructure Action under Contract RII3-CT-2004-506008 from the FP6 "Structuring the European Research Area Programme."

REFERENCES

1. Wreck-Reichhart, D., and Feyereisen, R. (2000) *Genome Biol.* **1,** 3003.1–3003.9
2. Davydov, D. R., Fernando, H., Baas, B. J., Sligar, S. G., and Halpert, J. R. (2005) *Biochemistry* **44,** 13902–13913
3. Lamb, D. C., Waterman, M. R., Kelly, S. L., and Guengerich, F. P. (2007) *Curr. Opin. Biotechnol.* **18,** 504–512
4. Pylypenko, O., and Schlichting, I. (2004) *Annu. Rev. Biochem.* **73,** 991–1018
5. Isin, E. M., and Guengerich, F. P. (2008) *Anal. Bioanal. Chem.* **392,** 1019–1030
6. Poulos, T. L., and Johnson, E. F. (2005) in *Cytochrome P450s: Structure Mechanism and Biochemistry* (Ortiz de Montellano, P. R., ed) 3rd Ed., pp 377–530, Kluwer Academic/Plenum Publishers, New York
7. Denisov, I. G., Makris, T. M., Sligar, S. G., and Schlichting, I. (2005) *Chem. Rev.* **105,** 2253–2277
8. Guengerich, F. P. (2008) *Chem. Res. Toxicol.* **21,** 70–83
9. Wienkers, L. C., and Heath, T. G. (2005) *Nat. Rev. Drug Discov.* **4,** 825–833
10. Williams, J. A., Hyland, R., Jones, B. C., Smith, D. A., Hurst, S., Goosen, T. C., Peterkin, V., Koup, J. R., and Ball, S. E. (2004) *Drug Metab. Dispos.* **32,** 1201–1208
11. Khosla, C., Tang, Y., Chen, A. Y., Schnarr, N. A., and Cane, D. E. (2007) *Annu. Rev. Biochem.* **76,** 195–221
12. Lambalot, R. H., Cane, D. E., Aparicio, J. J., and Katz, L. (1995) *Biochemistry* **34,** 1858–1866
13. Stassi, D., Donadio, S., Staver, M. J., and Katz, L. (1993) *J. Bacteriol.* **175,** 182–189
14. Chen, Y., Deng, W., Wu, J., Qian, J., Chu, J., Zhuang, Y., Zhang, S., and Liu, W. (2008) *Appl. Env. Microbiol.* **74,** 1820–1828
15. Savino, C., Sciara, G., Miele, A. E., Kendrew, S. G., and Vallone, B. (2008) *Protein Pept. Lett.* **15,** 1138–1141
16. Otwinowski, Z., and Minor, W. (1997) *Methods Enzymol.* **276,** 307–326
17. Leslie, A. G. W. (1992) *Joint CCP4/ESF-EACBM Newsl. Prot. Crystallogr.* **26,** 27–33
18. Collaborative Computational Project, N.4 (1994) *Acta Crystallogr. D Biol. Crystallogr.* **50,** 7690–7763
19. Vagin, A., and Teplyakov, A. (1998) *Acta Crystallogr. D Biol. Crystallogr.* **54,** 400–402
20. Cupp-Vickery, J. R., and Poulos, T. L. (1995) *Nat. Struct. Biol.* **2,** 144–153
21. Pannu, N. S., Murshudov, G. N., Dodson, E. J., and Read, R. J. (1998) *Acta Crystallogr. D Biol. Crystallogr.* **54,** 1285–1294
22. Laskowski, R. A., Moss, D. S., and Thornton, J. M. (1993) *J. Mol. Biol.* **231,** 1049–1067
23. Shindyalov, I. N., and Bourne, P. E. (1998) *Protein Eng.* **11,** 739–747
24. Koshland, D. E., Jr., Némethy, G., and Filmer, D. (1966) *Biochemistry* **5,** 365–385
25. Monod, J., Wyman, J., and Changeux, J. P. (1965) *J. Mol. Biol.* **12,** 88–118
26. Gotoh, O. (1992) *J. Biol. Chem.* **267,** 83–90
27. Li, H., and Poulos, T. L. (1995) *Acta Crystallogr. D Biol. Crystallogr.* **51,** 21–32
28. Ravichandran, K. G., Boddupalli, S. S., Hasermann, C. A., Peterson, J. A., and Deisenhofer, J. (1993) *Science* **261,** 731–736
29. Sherman, D. H., Li, S., Yermalitskaya, L. V., Kim, Y., Smith, J. A., Waterman, M. R., and Podust, L. M. (2006) *J. Biol. Chem.* **281,** 26289–26297
30. Cheng, G., Qian, B., Samudrala, R., and Baker, D. (2005) *Nucleic Acids Res.* **33,** 5861–5867
31. Heringa, J., and Argos, P. (1999) *Proteins* **37,** 44–55
32. Meunier, B., de Visser, S. P., and Shaik, S. (2004) *Chem. Rev.* **104,** 3947–3980
33. Pacey, M. S., Dirlam, J. P., Geldart, R. W., Leadlay, P. F., McArthur, H. A., McCormick, E. L., Monday, R. A., O'Connell, T. N., Staunton, J., and Winchester, T. J. (1998) *J. Antibiot.* **51,** 1029–1034
34. Ruan, X., Pereda, A., Stassi, D. L., Zeidner, D., Summers, R. G., Jackson, M., Shivakumar, A., Kakavas, S., Staver, M. J., Donadio, S., and Katz, L. (1997) *J. Bacteriol.* **179,** 6416–6425
35. Poulos, T. L., Finzel, B. C., and Howard, A. J. (1987) *J. Mol. Biol.* **195,** 687–700
36. Schlichting, I., Berendzen, J., Chu, K., Stock, A. M., Maves, S. A., Benson, D. E., Sweet, R. M., Ringe, D., Petsko, G. A., and Sligar, S. G. (2000) *Science* **287,** 1615–1622
37. Bell, S. G., Hoskins, N., Xu, F., Caprotti, D., Rao, Z., and Wong, L. L. (2006) *Biochem. Biophys. Res. Commun.* **342,** 191–196
38. Bell, S. G., Xu, F., Forward, I., Bartlam, M., Rao, Z., and Wong, L. L. (2008) *J. Mol. Biol.* **383,** 561–574
39. Davydov, D. R., Botchkareva, A. E., Kumar, S., He, Y. Q., and Halpert, J. R. (2004) *Biochemistry* **43,** 6475–6485
40. Yun, C. H., Song, M., Ahn, T., and Kim, H. (1996) *J. Biol. Chem.* **271,** 31312–31316
41. Bah, A., Garvey, L. C., Ge, J., and Di Cera, E. (2006) *J. Biol. Chem.* **281,** 40049–40056
42. Gianni, S., Ivarsson, Y., Bah, A., Bush-Pelc, L. A., and Di Cera, E. (2007) *Biophys. Chem.* **131,** 111–114
43. Fersht, A. R. (1999) *Structure and Mechanism in Protein Science,* Freeman, New York
44. Isin, E. M., and Guengerich, F. P. (2006) *J. Biol. Chem.* **281,** 9127–9136
45. Isin, E. M., and Guengerich, F. P. (2007) *J. Biol. Chem.* **282,** 6863–6874
46. Davydov, D. R., and Halpert, J. R. (2008) *Expert Opin. Drug Metab. Toxicol.* **4,** 1523–1535
47. Desai, R. P., Rodriguez, E., Galazzo, J. L., and Licari, P. (2004) *Biotechnol. Prog.* **20,** 1660–1665
48. Emsley, P., and Cowtan, K. (2004) *Acta Crystallogr. D Biol. Crystallogr.* **60,** 2126–2132

Investigating the Structural Plasticity of a Cytochrome P450: THREE-DIMENSIONAL STRUCTURES OF P450 EryK AND BINDING TO ITS PHYSIOLOGICAL SUBSTRATE

Carmelinda Savino, Linda C. Montemiglio, Giuliano Sciara, Adriana E. Miele, Steven G. Kendrew, Per Jemth, Stefano Gianni and Beatrice Vallone

J. Biol. Chem. 2009, 284:29170-29179.
doi: 10.1074/jbc.M109.003590 originally published online July 22, 2009